Sonocrystallization of interesterified fats with 20 and 30% of stearic acid at the sn-2 position and their physical blends

Journal:	*Journal of the American Oil Chemists Society*
Manuscript ID	JAOCS-17-0091.R1
Manuscript Type:	Original Article
Date Submitted by the Author:	n/a
Complete List of Authors:	Kadamne, Jeta; Utah state University, Department of Nutrition, Dietetics and Food Science Ifeduba, Ebenezer A.; Parabel USA, Inc., R&D Akoh, Casimir; University of Georgia, Food Science & Technology; Martini, Silvana; Utah State University, Department of Nutrition and Food Sciences
Keywords:	Fats and oils, Structure - Functional Properties < Food and Feed Science / Nutrition and Health, Fat crystallization < Lipid Chemistry / Lipid Analysis, Fractionation < Lipid Chemistry / Lipid Analysis, Interesterification < Lipid Chemistry / Lipid Analysis, Rheology < Lipid Chemistry / Lipid Analysis, Thermal Analysis < Lipid Chemistry / Lipid Analysis, Lipids

Sonocrystallization of interesterified fats with 20 and 30% of stearic acid at the sn-2 position and their physical blends

Jeta V. Kadamne[1], Ebenezer A. Ifeduba[2], Casimir C. Akoh[2], and Silvana Martini*[1]

[1]Department of Nutrition, Dietetics and Food Science, Utah State University, Logan, Utah 84322

[2]Department of Food Science and Technology, University of Georgia, Athens, Georgia 30602

*To whom correspondence should be addressed:

Silvana Martini

Department of Nutrition, Dietetics, and Food Science, Utah State University, 8700 Old Main Hill, Logan, Utah 84322

Phone: 435-797-8136

Fax: 435-797-2379

E-mail: Silvana.martini@usu.edu

ABSTRACT

Physical blends (PB) of high oleic sunflower oil and tristearin with 20 and 30% stearic acid and their interesterified (IE) products with 20 and 30% of the fatty acids being stearic acid at the *sn*-2 position were crystallized without and with application of high intensity ultrasound (HIU). IE samples were crystallized at supercoolings (ΔT) of 12, 9, 6, and 3 °C while PB were crystallized at ΔT = 12 °C. HIU induced crystallization in PB samples but not in the IE ones. Induction in crystallization with HIU was also observed at ΔT = 6 and 3 °C for IE C18:0 20% and 30% and at ΔT = 9 °C only for the 30% samples. Smaller crystals were obtained in all sonicated samples. Melting profiles showed that HIU induced crystallization of low melting triacylglycerols (TAGs) and promoted co-crystallization of low and high melting TAGs. In general, HIU significantly changed the viscosity, G', and G'' of the IE 20% samples except at ΔT = 12 °C. While G' and G'' of IE 30% did not increase significantly, the viscosity increased significantly at ΔT = 9, 6, and 3 °C from 1,526 ± 880 to 6,818 ± 901 Pa.s at ΔT = 3 °C. The improved physical properties of the sonicated IE can make them good contenders for *trans*-fatty acids replacers.

Keywords: Interesterified fats, physical blends, physical properties, crystallization, rheology, melting, ultrasound

INTRODUCTION

Modification of the physical properties of fats is often desired to obtain specific functionalities for use in various food applications. Enzymatic interesterification is a widely used processing technique to achieve this [1]. Interesterification changes the triacylglycerol (TAG) composition of the fat without changing its fatty acid composition [2]. In 2016 Ifeduba et al. [3] enzymatically interesterified physical blends of (a) high oleic sunflower oil (HOSO) and tripalmitin and (b) HOSO and tristearin to develop fats containing TAGs with palmitic or stearic acid at the *sn*-2 position. Several studies have evaluated the effect of IE fats consumption with saturated fatty acids at the *sn*-2 position. Results from these studies are variable and no consensus about the nutritional properties of these IE fats has been achieved. However, some studies show that TAGs with saturated fats at the *sn*-2 position can either reduce [4, 5] or have no effect on postprandial lipemia [6, 7]. Increasing uses of interesterification by the lipid industry and consumer demands for healthier fats prompts the need of exploring the functionalities and physical properties of these new fats. Changes in TAG composition of fats upon interesterification affects their crystallization behavior [8] and depending on the new TAGs formed, the resulting IE fats could have slower crystallization behavior than their corresponding physical blends (PB) [9]. Therefore, IE fats are in general softer than their PB counterparts and the interesterification process limits their uses in many foods where harder fats are needed.

Extensive research has been performed related to the use of high intensity ultrasound (HIU) to induce crystallization of ice [10], sucrose [11] and fats such as cocoa butter [12], anhydrous milk fat [13, 14], palm kernel oil [13] and interesterified soybean oil [15]. HIU has been shown to change the crystallization behavior of lipids by inducing and accelerating the formation of smaller [15] and more fat crystals [14], creating harder fats [13], increasing

viscosity [14, 16], viscoelastic properties [15] and solid fat content [17]. Choosing appropriate sonication conditions such as size of the sonicator tip, amplitude of sonication, duration, crystallization temperature and amount of crystallizing material is essential for improved results [15, 17]. However, the role that fat chemical composition plays on lipid sonocrystallization still remains unknown.

The authors of this paper previously studied the crystallization behavior of interesterified (IE) fats with palmitic acid at the *sn*-2 position and the corresponding physical blends [18]. This study allowed us to compare the crystallization behavior of fats with similar fatty acids but different TAG composition along with the comparison of fats with different content of saturated fatty acids (SFA). The palmitic containing IE fats were found to be softer than their physical blends and the hardness of the IE samples was increased by using HIU. In the present study, the tripalmitin previously used by Kadamne et al. [18] in the PB was replaced by tristearin with the assumption that the higher melting stearin in the corresponding IE will provide a harder texture compared to the palmitic containing IE. Using interesterification conditions reported in Ifeduba et al. [3] IE fats with low total saturated fatty acids (20-30%) and stearic acid at the *sn*-2 position were produced.

The objective of this research is to evaluate the crystallization behavior of the IE fats containing 20 and 30% stearic acid at the *sn*-2 position and of the physical blends used to synthesize these IE samples. The effect of HIU on their crystallization behavior was studied at different supercooling levels. Crystal microstructure, solid fat content, viscosity, elastic and storage modulus, and melting behavior were evaluated. The fats used in this study differ from those in the previous study based on the major saturated fatty acid at the *sn*-2 position, which is stearic acid in the present and palmitic acid in the former [18]. Along with the characterization of

the physical properties of the IE fats, these studies will help us to understand the effectiveness of ultrasound-induced crystallization with changes in type and amount of SFA.

MATERIALS AND METHODS

Starting Materials. Dr. Akoh's laboratory from the University of Georgia provided the interesterified (IE) and physical blends (PB) of tristearin (>99% purity, Spectrum Chemicals, Gardena, CA) and high oleic sunflower oil (Stratas Foods, Memphis, TN). The two PB samples contained a total of 20 and 30% stearic acid while in the IE prepared by the interesterification of PB using Lipozyme TLIM [3], among the fatty acids at the *sn-2* position, about 20 and 30% were occupied by stearic acid. . The PB used to prepare the IE samples containing 20% stearic acid at the *sn*-2 position (IE C18:0 20%) will be referred to as PB C18:0 20% while the physical blends used to prepare the IE samples containing 30% stearic acid at the *sn*-2 position (IE C18:0 30%) will be referred to as PB C18:0 30%.

Melting point determination: The IE and PB samples were melted completely upon reception, filtered while hot to remove any foreign impurity and stored at -20 °C until further use. The AOCS Official Method Cc 1-25 was used to measure the melting point of the IE and PB samples.

Fatty acid analysis and triacylglycerol composition: The samples were analyzed for their fatty acid composition and triacylglycerol content according to the methods outlined by Ifeduba et al. [3].

Crystallization experiment. Crystallization experiments were performed in a double wall glass cell with an external water bath to control the sample temperature. A magnetic stirrer was used to provide agitation at 100 RPM. Thirty grams of filtered sample was melted in the microwave and

later kept in the oven at 100 °C for 45 min to remove crystal memory. The melted sample was then placed in the crystallization cell. Crystallization was performed at supercooling levels (ΔT) of 12, 9, 6, and 3 °C. Crystallization temperatures (T_c) used for each sample at each supercooling are shown in Table 1. The crystallization behavior of the samples was monitored using a He-Ne laser source (105-2 Uniphase, San Jose, CA) as previously described by Wagh et al. [19]. The temperature of the sample was monitored by the thermocouple along with the laser signals and recorded by LabVIEW 8.0 software (National Instruments Corp., Austin, TX). Sonication was performed using a Misonix 3000 sonicator (20 kHz, Misonix Inc., Farmingdale, NY) and 3.2 mm diameter tip operating at 216 μm vibration amplitude for 5 s.

Prior to crystallization, the experimental set up was set at the desired temperature along with the sonication equipment with the stirrer. The position of the laser was arranged such that a maximum laser signal output of 10 V was obtained through the empty cell. After the sample was introduced in the crystallization cell, the laser signal was monitored. The laser signal remained at its highest value until the sample started to crystallize. At this point, the laser signal decreased steadily. When the laser signal reached a value of 0.6 V, which corresponds to a slight amount of turbidity in the media, the agitation was stopped and HIU was applied to the sample. The 0.6 V laser output was chosen as the time point for HIU application since it corresponds to a slight turbidity indicative of the onset of crystallization. This allows for consistent sonication conditions for all the samples. Immediately after sonication, the sample was transferred into five nuclear magnetic resonance (NMR) tubes and three centrifuge tubes which were pre-warmed at the crystallization temperature and kept in the water bath until 60 min from the start of the experiment. The NMR tube samples were used to measure solid fat content (SFC) while the samples in the centrifuge tubes were used for microscopy, melting characteristics, and rheology.

If the Laser signal reached 0.6 V after 10 min of crystallization, the agitation was stopped at 10 min and the sample was crystallized further without agitation.

Samples evaluated in this study were crystallized without and with sonication. The non-sonicated samples were transferred to the tubes immediately after the laser signal reached 0.6 V. The crystallization experiment at each processing condition was performed in triplicates and the analyses were performed once after each of the triplicate runs.

Solid fat content. The five NMR tubes were kept in the water bath and the SFC of the sample in tube was measured every 2 min until 60 min of crystallization using Minispec mq20 (Bruker Biospin GmbH, Rheinstetten, Germany). The measurement of SFC started after the laser signal reached 0.6 V. For the sake of curve fitting, SFC points of 0% SFC were added to time point prior to the start of measurement. The tubes were put back into the water bath after SFC was measured and the tubes were used in rotation for further time points. The mean SFC values along with their standard error were plotted against time and the reparametrized Gompertz equation [20] was fitted to the data. Equation 1 shows the reparametrized Gompertz equation.

$$s(t) = s_{\max} \times e^{\left\{ e^{-\left(\frac{\mu_{\max} \times e}{s_{\max}} x(\lambda - t) + 1 \right)} \right\}} \quad (1)$$

Where $s_{(t)}$ is the % SFC at time t, s_{max} is the maximum SFC, μ_{max} is the maximum growth rate (% SFC/min), λ is the induction time of crystallization (min), e = 2.718281 [20].

Polarized light microscopy. Sample aliquots were taken from the centrifuge tube in the water bath every 10 min until 60 min of crystallization using pre-warmed glass pipettes and placed onto glass slides and then covered with cover slides. The microstructure of the sample was observed by the Olympus BX41 polarized light microscope (PLM) (Olympus, Tokyo, Japan) at

10X magnification. The microscope was fitted with an Instec TS62 thermal stage (Instec, Inc., Boulder, CO) that was set to the crystallization temperature to prevent any change in the crystallization conditions in the slides due to temperature fluctuations.

Differential scanning calorimetry. The melting behavior of the samples was analyzed after 60 min of crystallization by a DSC Q20 (TA Instruments, New Castle, DE). The sample was sealed hermetically in a Tzero pan with a Tzero hermetic lid and heated in the DSC from the crystallization temperature to 80 °C at 5 °C/min. The melting peaks were integrated to quantify the peak melting temperature (T_p), onset temperature of melting (T_{on}) and the melting enthalpy (ΔH). For the calculation of the driving force of crystallization, the melting enthalpies were calculated by equilibrating the sample in the hermetically sealed pans overnight at -20 °C and followed by heating in the DSC from -20 C to 80 °C at 5 °C/min. The driving force for the crystallization of fats can be calculated using equation 2:

$$\phi = \frac{\Delta H \times \Delta T}{Tm} \qquad (2)$$

where ΔH is the change in enthalpy associated with the melting (J/g); ΔT is the supercooling (°C); and T_m is the melting point of the sample (°C).

Rheology. Rheological parameters including viscosity, storage (G') and loss (G'') moduli and the phase angle (δ) were measured using a AR-G2 Rheometer (TA Instruments, New Castle, Delaware). The viscosity was measured by a steady state flow procedure by increasing the shear rate from 0.01 to 300 (s^{-1}) at the crystallization temperature. Sample viscosity at 0.1 s^{-1} shear rate was reported. The measurement of the viscoelastic parameters (G', G" and δ) was performed at T_c by a strain sweep oscillation procedure where the strain values changed from 0.008 to 10% at constant frequency of 1 Hz.

The rheological parameters of the IE samples were measured using a parallel plate geometry (40 mm diameter) using samples from the centrifuge tubes in the water bath after being 60 min at T_c. The PB had a crumbly texture and therefore these samples were transferred to 20 mm diameter molds after the laser reached 0.6 V to obtain a more uniform network. The molds were maintained at T_c for the duration of the experiment (60 min). The samples from the molds were used to measure the rheological parameters of the PB samples using parallel plate geometry (20 mm diameter). The rheology data was collected after each of the three separate runs at each processing condition. Thus the rheological data was collected and presented as the mean of the triplicate values along with its standard error of the mean.

Statistical Analysis. At $\Delta T = 12$ ºC IE and the PB samples were compared within each fatty acid content using a two-way ANOVA followed by Tukeys' post hoc test at $\alpha = 0.05$. Results for IE C18:0 20% samples at $\Delta T = 9$, 6, and 3 ºC were compared using a two-way ANOVA followed by the Sidak's multiple comparison test to compare the effect of sonication at each supercooling level. Similar statistics were performed for the IE C18:0 30% samples at $\Delta T = 9$, 6, and 3 ºC.

RESULTS AND DISCUSSION

Melting point. The melting point of the PB C18:0 20% sample was 53.6 ± 0.4 °C while that of the IE C18:0 20% sample was 38.0 ± 0.3 °C. The PB C18:0 30% and IE C18:0 30% sample had melting points of 60.0 ± 0.4 and 43.2 ± 0.6 °C, respectively (Table 1). The melting point decreased upon interesterification due to the decrease in the amount of tristearin in the samples while the samples containing 30% stearic acid had a higher melting point than the 20% samples due to their higher percentage of stearic acid.

Fatty acid composition. The fatty acid composition of the PB samples was reported earlier by Ifeduba et al. [3]. The major fatty acids, oleic and stearic acid were present at 68.1 and 21.0% level in the PB C18:0 20% and at 58.8 and 30.1% level in the PB C18:0 30%. In the PB C18:0 20% and the 30% samples, 11.7 and 19.8 % respectively, of the fatty acids at the *sn-2* position were occupied by stearic acid.

The total and *sn*-2 fatty acid composition of the IE samples is presented in Table 2. Oleic acid from the high oleic sunflower oil starting material was the highest in the IE sample and was present at 70.2 and 60.7% in the IE C18:0 20 and 30% sample, respectively. The next fatty acid in the highest concentration was stearic acid, derived from the tristearin starting material and the total level of stearic acid in the IE C18:0 20% and 30% samples was 19.2 and 28.3%, respectively. In the IE C18:0 20% and 30% samples, 17.0 and 33.2% respectively of the fatty acids at the *sn-2* position were occupied by stearic acid. The major fatty acid at the *sn*-2 position was oleic acid and was present at 75.2% and 60.0% in the 20 and 30% samples, respectively.

Triacylglycerol composition. The TAG composition of the PB samples has been discussed elsewhere [3]. The major TAGs in the PB C18:0 20% were OOO (79.4%) and SSS (11.4%) and the corresponding levels of these TAGs in the PB C18:0 30% sample were 68.5 and 22.3%, respectively [3]. The TAG composition of the IE samples is presented in Table 3. Upon interesterification, SSS in the PB C18:0 20% samples changed from 11.4% to 1.2% and the OOO decreased from 79.4 to 69.0%. New TAG species were formed in the IE samples including OOS and OSS at 23.7 and 4.0% levels, respectively. The amount of SSS, OOO, OOS and OSS in the IE C18:0 30% was 2.3, 39.9, 42.7 and 14.3%, respectively. Lower content of SSS (1.2%), OSS (4.0%), OOS (23.7%) while higher contents of OOO (69.0%) and LOO/LPO (2.1%) were obtained for the IE C18:0 20%.

Solid fat content. In order to compare the results with our previous study [18], the samples from these study were crystallized at supercoolings of 9, 6, and 3 ºC. However, at these supercoolings, the physical blends did not crystallize into a uniform crystalline network that allowed the characterization of its physical properties. The PB was rich in SSS and OOO which have melting points of 73.5 and 4.5-5.7 °C, respectively [21]. Due to large differences in the melting points of these TAGs, the PB crystallized in two separate fractions: the stearin and the olein fraction and did not form a continuous network of crystals. Due to this discontinuous network, the laser signal did not drop as expected and hence similar crystallization conditions could not be generated in the PB at different supercooling levels. Hence, the samples were also crystallized at ΔT = 12 ºC where the PB did not fractionate and generated a turbid crystalline sample which reproducibly decreased the laser signal over time. Thus, the IE were crystallized at 4 supercooling levels while the PB was crystallized at only ΔT = 12 ºC. The solid fat content (SFC) of the IE and PB samples at ΔT = 12 ºC are shown Figure 1, while the SFC of IE samples at supercoolings of 9, 6, and 3 ºC are shown in Figure 2. The time point of application of HIU is shown by an arrow pointing at the time axis. The SFC data was fitted to the Gompertz equation as described in the Materials and Methods section above (equation 1) and the parameters obtained are tabulated in Table 4. The maximum SFC, s_{max}, of PB crystallized at ΔT = 12 ºC was higher than that of the IE samples for both the C18:0 20 and 30% samples (Figure 1, Table 4) ($p < 0.05$). When samples were crystallized without sonication the s_{max} of the PB C18:0 20% sample was 13.5% while that of the IE C18:0 20% sample was 8.6%. Similarly, the s_{max} of the PB C18:0 30% sample was 18.2% while that of the IE C18:0 30% sample was 10.8%. Application of HIU to the PB samples did not induce crystallization in the 20% (Figure 1A) while an induction was observed for the 30% ones (Figure 1B). A significant ($p < 0.0001$) decrease in the induction period of

crystallization (λ) was observed for the sonicated PB C18:0 30% sample from 11.9 to 8.7 min and an increased growth rate from 3.2 to 4.8 % SFC/min (Table 4). The maximum growth rate (μ_{max}) of the PB C18:0 20% samples increased significantly ($p < 0.05$) from 3.33 to 10.12 % SFC/min even though there was no significant change in the induction period of crystallization (Table 4) ($p > 0.05$). At $\Delta T = 12$ ºC, HIU did not affect the crystallization kinetics of IE samples (Figure 1A, 1B, and Table 4). Based on the similarity in the isothermal SFC curves of the IE samples at $\Delta T = 12$ ºC (Figure 1A, B) and no the lack of difference in the crystallization kinetics upon sonication (Table 4) it can be concluded that at $\Delta T = 12$ ºC supercooling and not sonication was the dominant force that drove the crystallization of IE samples. In general, the s_{max} of the IE C18:0 30% samples were higher than those of IE C18:0 20% samples (Figure 1A and 1B, Table 4). This can be due to the higher stearic acid content and the slightly higher content of SSS in the 30% samples.

HIU induced crystallization in the IE C18:0 20% samples at supercooling of 6 and 3 ºC and significantly decreased the λ from 9.36 to 8.39 min at $\Delta T = 6$ ºC ($p < 0.05$) and from 13.03 to 11.77 min at $\Delta T = 3$ ºC ($p < 0.05$). HIU also significantly increased the rate of crystallization from 0.76 to 1.61 at $\Delta T = 6$ ºC and from 0.46 to 1.54% at $\Delta T = 3$ ºC (Table 4) ($p < 0.05$). Sonication also induced crystallization in IE C18:0 30% samples at supercoolings of 9, 6, and 3 ºC. The maximum growth rate (μ_{max}) increased significantly ($p < 0.0001$) from 0.66 to 1.38 % SFC/min at $\Delta T = 9$ ºC upon sonication and the effect was also observed at the lower supercoolings (Figure 2 D, Table 4). Although the s_{max} of IE C18:0 30% samples slightly increased with sonication at $\Delta T = 9$, 6, and 3 ºC, the increase was not statistically significant ($p > 0.05$). In addition, the induction period of crystallization decreased significantly ($p < 0.0001$) only for $\Delta T = 3$ ºC from 29.3 to 21.4 min (Figure 2F, Table 4). Similar results were obtained in

the previous study with IE C16:0 30% samples at ΔT = 3 ºC where even though no significant increase in the s_{max} was observed with sonication, the induction period of crystallization decreased from 34.4 min to 26.8 min [18].

The crystallization behavior observed at the different supercoolings can be explained based on the driving force of crystallization reported in Table 1. The enthalpy of melting used to calculate the driving force of crystallization was measured using the DSC and were 105.2 and 106.5 J/g for the PB and IE C18:0 20% samples and 126.4 and 105.2 J/g for the PB and IE C18:0 30% samples (Table 1). Thus, based on Eq. 2, for a specific sample, high supercoolings can be obtained by lowering the crystallization temperature, thereby creating a higher driving force for crystallization. As the driving force increased, there was an induction in the crystallization of the samples. For example, at ΔT = 12 ºC the driving force for the non-sonicated IE C18:0 20% was 33.6 J/g (Table 1) and the induction period of crystallization was approximately 2 min (Table 4) while at subsequent supercoolings of 9, 6, and 3 ºC, the induction period increased to 4, 9.4 and 13 min, respectively (Table 4) due to the decreasing driving force of 25.2, 16.8 and 8.4 J/g (Table 1). The driving forces for the 30% stearic samples were lower, but in the same order of magnitude, than the corresponding 20% stearic samples for the same supercooling. This was due to the similar melting enthalpy and the higher melting point of the C18:0 30% samples. The driving force for the IE C18:0 30% samples at supercoolings of 12, 9, 6 and 3 ºC were 29.2, 21.9, 14.6 and 7.3 J/g, respectively (Table 1) and the corresponding induction period of non-sonicated crystallization were 2.2, 9.4, 15.5 and 29.3 min, respectively (Table 4). The driving force of the IE C18:0 30% samples was lower compared to the IE C18:0 20%. It took longer for the IE C18:0 30% samples to crystallize compared to the IE C18:0 20% samples at all the

supercoolings. The PB samples had lower driving force than the corresponding IE samples and hence the induction period of the PB was higher than those of the IE at ΔT = 12 ºC.

At ΔT = 9 ºC, the driving force of the IE C18:0 20% sample was 25.2 J/g and based on the SFC curves in Figure 2A it can be seen that there was no difference in the crystallization kinetics of the sonicated and non-sonicated sample. This suggests that similar to the IE samples at ΔT = 12 ºC, the supercooling dominated crystallization of IE C18:0 20% sample at 9 ºC and sonication had no effect on the induction of crystallization. However, for the PB C18:0 30% sample at ΔT = 12 ºC, the driving force was 25.3 J/g and HIU induced crystallization despite the high driving force. This was due to the greater percentage of the higher melting SSS fraction. The cavitation generated by the HIU induced secondary crystallization of the SSS in the supercooling PB sample. Induction in the crystallization of the SSS was not observed at ΔT = 9 ºC in the IE C18:0 20% sample due to the low amount of SSS compared to the PB C18:0 30% sample.

The s_{max} of the samples was higher with higher driving force in the case of IE samples. However, the s_{max} of the PB samples was higher than the IE samples, even though the driving force of the IE was higher. This suggests that the driving force of crystallization was an important factor for the induction of crystallization. However, the composition of the fat played a bigger role in the overall SFC of the fat samples. In the case of the PB samples, the higher SSS content induced a higher s_{max} in the PB samples and higher content of SSS in IE C18:0 30% compared to IE C18:0 20% resulting in higher s_{max}.

Compared to the previous crystallization studies by the current authors [18], the IE samples with 20% palmitic acid at the *sn*-2 position crystallized in two steps while the stearic samples crystallized in a single step. The driving force for the IE C16:0 20% sample was 39.68 J/g while that for the IE C18:0 20% sample was 25.2 J/g at 9 ºC supercooling level. The lower driving

force obtained in the stearic sample for the same degree of supercooling may have allowed sufficient time for the low and high melting TAGs to crystallize together and evidenced as a single-step growing curve. The IE C16:0 30% sample also crystallized in two steps at $\Delta T = 9$ ºC for the palmitic-based samples. However, similar to the IE C18:0 30% samples, due to the decrease in the driving force, with lower supercoolings, the IE C16:0 30% crystallized in a single step. The μ_{max} and the $s_{max.}$ of the IE C18:0 samples were higher than those of the IE C16:0 samples [18] and these differences can be attributed to the presence of the higher melting TAGs in the samples in the current study. Interestingly, sonication did not induce crystallization of samples with 20% of C16:0 for any of the supercooling levels tested but did have an effect on the crystallization of samples with 20% C18:0. Similar to the previous discussion, the presence of C18:0 with a higher melting point than C16:0 might be responsible for this different effect.

Microstructure. Crystal microstructures obtained for the PB and IE samples crystallized at $\Delta T =$ 12 ºC after 60 min of crystallization are presented in Figure 3. The bright structures in the picture represent the crystals while the dark background represent the liquid part. Upon visual comparison, the PB had larger crystals than the IE samples. Small and large number of crystals were present in the microstructure of the IE C18:0 20% sample without and with sonication. Similar to the SFC, sonication did not affect the microstructure of IE C18:0 20% at the highest supercooling. The crystal size of the IE C18:0 30% seemed larger than those obtained for the IE C18:0 20% samples. The induction period of crystallization of the IE C18:0 30% samples were slightly higher than those of the IE C18:0 20% samples. This provided more time for the TAGs to rearrange and hence the crystals of the IE C18:0 30% were slightly larger than the IE C18:0 20% samples. Based on the induction of secondary nucleation caused by HIU slightly smaller crystals were observed in the sonicated IE C18:0 30%. Although there was a change in the

microstructure of the sample, there was no change in the SFC of the sample. The crystals of PB C18:0 30% were larger than all the samples at ΔT = 12 ºC and smaller crystals were observed in sonicated PB C18:0 20% and 30% samples.

From Figure 4, it can be seen that there was formation of smaller crystals in the IE C18:0 20% samples upon sonication at supercoolings of 9, 6, and 3 ºC. Although the amount of crystals did not decrease with the decrease in supercooling, slightly larger crystals can be seen in non-sonicated samples at the lowest supercooling. When compared to the previous study involving samples containing 20 and 30% palmitic acid at the *sn*-2 position [18], the IE C16:0 20% samples had fewer crystals compared to the IE C18:0 20% samples. With decreasing supercooling, there was a decrease in the amount of crystals in the IE C16:0 20% samples while in the case of IE C18:0 20% samples, the decrease in the supercooling increased the size of the crystals while there was no visible change in the amount of crystals in the microstructure. Although HIU application induced the formation of smaller crystals in the IE C18:0 20% sample at all the supercoolings, the HIU was not as effective in the case of the IE C16:0 20% samples. These results correlate well with the higher SFC of the IE C18:0 20% samples (5.5% and 5.6% for non-sonicated vs. sonicated samples, respectively at ΔT = 3 ºC) compared to the IE C16:0 20% samples from the previous study [18] (3.8% and 3.6% for non-sonicated vs. sonicated samples, respectively at ΔT = 3 ºC).

The microstructure of the IE C18:0 30% samples at ΔT = 9, 6, and 3 ºC are presented in Figure 5. Compared to the ΔT = 12 ºC, slightly larger crystals were formed in the non-sonicated samples at all supercoolings. Similar results were observed by Herrera et al. [22] and Martini et al. [23] in milk fat and, milk fat fractions and sunflower oil blends, respectively. According to Martini et al. [23] at low supercoolings, or at a higher crystallization temperature, fewer nuclei

were formed. This condition favors the growth of the already formed nuclei resulting in fewer and bigger crystals. HIU induced smaller and more crystals in IE C18:0 30% at all the supercoolings. Compared to the previous study with palmitic samples [18], at ΔT = 3 ºC, higher amount of crystals can be seen in the stearic samples and this correlates well with the higher SFC of these samples at the end of crystallization. IE C18:0 30% samples had SFC values of 5.2% and 5.6% for the non-sonicated and sonicated samples, respectively; the IE C16:0 30% had SFC values of 3.4% and 4.5% for the non-sonicated and sonicated samples, respectively. Increase in the number of smaller crystals upon sonication has been reported previously by several authors [13-15, 17, 18, 24]. In the current study, HIU was applied in the presence of crystals similar to experimental conditions used by Suzuki et al. [13] and Ye et al. [15] According to Suzuki, HIU increased the amount of nuclei in the system by inducing secondary nucleation by breaking the existing nuclei in the system along with primary nucleation.

Differential scanning calorimetry. The melting thermograms of the IE and PB samples at ΔT = 12 ºC are shown in Figure 6 and the corresponding T_{on}, T_p and the enthalpy (ΔH) of melting of the samples are presented in Table 5. The PB C18:0 20% samples had a single peak for both the sonicated and the non-sonicated sample at ΔT =12 ºC with a peak melting temperature of 61.2 ± 0.4 ºC and 61.4 ± 0.1 ºC, respectively (Figure 6A, Table 5). The melting thermograms of the sonicated PB sample shows a shoulder next to the peak melting temperature which was absent in the non-sonicated sample (Figure 6A). This indicates that there was a slight induction in the crystallization of the lower melting components in the fat such as PSS (2.7%) or PPS+OPS (2.5%) [3]. The IE C18:0 20% samples had a T_p of 52.8 ± 0.1 and 52.7 ± 0.1 ºC with an enthalpy of 9.2 ± 0.5 and 9.4 ± 0.1 J/g without and with sonication, respectively. The majority of TAGs in the IE C18:0 20% sample were SSS (1.2%), OSS (4.0%), OOS (23.7) and OOO (69.0%). This

sample showed a single broad melting peak indicating that these TAGs co-crystallized (Figure 6A). Thus, HIU did not affect the crystallization behavior of the IE samples and this confirms the previous speculation that at a ΔT = 12 ºC, supercooling dominated the crystallization of the IE C18:0 20% samples.

The PB C18:0 30% samples had two well-defined melting peaks with the first peak melting temperatures of 58.1 ± 0.7 ºC and the second peak at 64.9 ± 0.5 ºC for the non-sonicated sample (Figure 6B, Table 5). The higher melting peak corresponds to the crystallization of the SSS TAG while the lower melting peak corresponds to crystallization of PSS (3.8%) and PPS+OPS (2.1%) [3]. For the non-sonicated and sonicated PB C18:0 30%, the melting enthalpy of the first peak was 21.9 ± 3.8 and 36.1 ± 7.1 J/g, respectively and that of the second peak was 10.8 ± 4.8 and 13.0 ± 5.3 J/g, respectively. The IE C18:0 30% sample at ΔT= 12 ºC also had two peaks in the melting thermograms (Figure 6B). The IE C18:0 30% sample had 2.3% SSS which drives the crystallization of the sample. The higher melting peak corresponds to the crystallization of SSS while the lower melting peaks may comprise of OSS, SOS, OOS and OSO. The other TAGs including OOO (melting point = 4.5-5.7 ºC), LOO (melting point 5.1 ºC), and LOP (melting point = 13.3 °C) had melting points below the crystallization temperature and do not contribute to the crystallization behavior of these samples. However, the changes in the enthalpy of melting in sonicated samples were not as drastic as compared to the ones observed in the PB sample indicating that sonication did not alter the crystallization of the samples.

The melting thermograms of the IE C18:0 20% and the 30% samples at supercoolings of 9, 6, and 3 ºC are shown in Figure 7A-F and the corresponding data is presented in Table 6. At ΔT = 9 ºC, IE C18:0 20% showed a single melting peak similar to the behavior observed at ΔT = 12 °C (Figure 6A). The peak melted at 53.1 ± 0.4 ºC and upon sonication, this peak had a lower melting

enthalpy that decreased significantly from 6.8 to 4.1 J/g ($p < 0.001$). Also, sonicated sample showed a shoulder peak at 41.2 ± 0.7 ºC with a low melting enthalpy of 0.8 J/g (Figure 7A, Table 6). Although it was observed that HIU did not affect the SFC or the microstructure at this supercooling, the DSC data suggests that sonication induced the crystallization of lower melting TAGs (OSS and SOS) at this supercooling which was not observed at ΔT = 12 ºC. This effect was even more prominent at ΔT = 6 ºC and a new peak was formed upon sonication at 44.7 ± 0.3 ºC which was not seen in the thermograms of the non-sonicated sample (Figure 7B, Table 6). The melting enthalpy of the low temperature peak was 4.9 J/g which was higher than the peak at ΔT = 6 ºC. At the lowest supercooling (ΔT = 3 ºC), sonication favored the crystallization of the lower melting fractions and decreased the size of the higher melting peak from an average enthalpy of 1.2 to 0.1 J/g (Figure 7C, Table 6). Although sonication did not affect the T_p, the T_p increased with the decrease in supercooling. This indicates that sonication did not fractionate the sample into new TAG fractions but favored the crystallization of the already crystallizing lower TAGs.

The non-sonicated IE C18:0 30% samples, on the other hand, crystallized in two fractions with peak melting temperatures of 45.2 ± 0.3 ºC and 54.5 ± 0.3 ºC at ΔT = 9 ºC (Figure 7D, Table 6). This behavior was similar to that observed for the sample crystallized at ΔT = 12 ºC (Figure 6). In general, upon sonication of the IE C18:0 30% samples, there was an increase in the enthalpy of the first peak while the enthalpy of the second peak decreased. Also, there was a significant increase in the T_p of the first peak indicating that HIU induced the co-crystallization of these two fractions ($p < 0.01$). At ΔT = 9 ºC, the IE C18:0 30% sample melted in two peaks with peak melting temperatures of 45.2 and 54.5 ºC (Figure 7D) and upon sonication, the enthalpy of the higher melting peak decreased from 2.6 to 0.1 J/g and the enthalpy of the first peak at 46.3 ºC

increased from 3.8 and 13 ºC (Table 6). Although a small second peak was seen at ΔT = 6 ºC in the thermograms of the IE C18:0 30% sample, this peak disappeared in the sonicated sample along with a slight increase in the enthalpy of the first peak from 11.3 to 12.9 J/g, although not statistically significant (Figure 7E, Table 6). At ΔT = 3 ºC there was only one peak in the sonicated and non-sonicated IE C18:0 30% melting thermograms (Figure 7F). However, there was a significant increase in the melting enthalpy of this peak from 9.4 to 12.9 J/g in the sonicated sample indicating that HIU induced crystallization (Table 6). This correlates well with the PLM data where a more crystalline material can be observed in the sonicated sample compared to the non-sonicated one.

The differences in the melting behavior of the IE C18:0 20% and the IE C18:0 30% samples can be explained based on the differences in the SSS content of the samples: 1.2 and 2.3% respectively. The thermograms of the IE C18:0 20% samples indicate that the higher driving force of the samples favored the crystallization of the higher melting TAG, SSS (1.2%) along with the OSS (4.0%). However, due to the lower amount of OSS, the lower melting peak was not as prominent. Upon sonication, secondary nucleation was induced and the crystallization along with the growth of OSS around these secondary nuclei was favored. As the temperature of crystallization increased, the system had sufficient time to allow for the crystallization of the lower melting TAGs. On the other hand, due to the higher concentration of SSS (2.3%) and OSS (14.3%) in the IE C18:0 30% sample at this supercooling, there were two peaks in the melting thermograms (Figure 7D). Similar to the IE C18:0 20% and the ability of the HIU to induce secondary crystallization, the crystallization of the OSS was favored and the T_p matched with the melting point of OSS (45 ºC). Also, in both the IE C18:0 20% and 30% samples HIU induced the crystallization of the lower melting TAGs (OSS) and promoted the incorporation of higher

melting point TAGs (SSS) into the crystalline network. This co-crystallization resulted in an increase in size of the first melting peak and a decrease in the size of the second melting peak.

Rheology. The rheological parameters of the IE and the PB samples at ΔT =12 ºC are presented in Figure 8. Viscosity and G' values of IE C18:0 20% samples were significantly higher than those observed in PB samples ($p < 0.05$) (Figure 8 A-B). Although the SFC of the PB samples was higher than the IE samples, the rheological parameters for the IE were an order of magnitude higher than the PB ones. The PB samples contained about 11.4% SSS which contributes to the majority of the SFC of the PB samples. However, it also contains 79.4% of OOO which had a melting point of 4.5-5.7 ºC and may be entrapped along with the SSS crystalline matrix. However, due to the big difference in the melting points of the TAG fractions in the PB samples, there may not be a uniform strong crystalline matrix. Hence, the overall rheological parameters were weaker than the corresponding IE samples which had TAG fractions such as OSS, OOS with melting points in the vicinity of each other and may have led to the co-crystallization of several TAG species together. The differences in the rheological properties can also be attributed to the differences in the microstructure of the samples. Based on the PLM pictures presented in Figure 3, it can be seen that the microstructure of the IE samples was comprised of smaller and more crystals compared to those of the PB samples. It has been shown before [15, 18] that smaller crystal microstructure increases the rheological properties of fats.

The viscosity of the non-sonicated PB C18:0 20% sample was 85 ± 37 Pa.s while that of the IE C18:0 20% sample was 736 ± 143 Pa.s at ΔT = 12 °C. The rheological parameters did not change upon sonication. This correlates well with the SFC and the PLM data. There was no change in the final SFC of either the IE or the PB samples with sonication due to the high supercooling. The PLM of the IE samples were also similar without and with HIU. Sonication

induced the formation of smaller crystals in PB microstructure which did increase the magnitude of the rheological parameters, but this increase was not statistically significant ($p > 0.05$).

On the other hand, the magnitude of the rheological parameters was higher for the PB C18:0 30% samples compared to the IE C18:0 30% samples. This may correspond to the higher SSS content (22.3%) in the PB C18:0 30% which was almost twice the amount in the PB C18:0 20% samples. Crystallization of this high melting TAG may have contributed to the rheological properties of the fat blend. The viscosity of the non-sonicated PB C18:0 30% sample was 19,430 ± 4,950 Pa.s while that of the IE C18:0 30% sample was 1,160 ± 201 Pa.s. Upon sonication, although there was induction of smaller crystals in the PB C18:0 30% samples (Figure 3), the viscosity significantly decreased to 2,481 ± 997 Pa.s ($p < 0.05$). However in the IE C18:0 30% samples, there were smaller crystals in the microstructure upon sonication at ΔT =12 ºC (Figure 3) and the viscosity of the sonicated sample was 2,963 ± 758 Pa.s. The G' and the G" of the PB C18:0 30% sample were $1.9 \times 10^6 \pm 4.9 \times 10^5$ Pa and $3.4 \times 10^5 \pm 9.1 \times 10^4$ Pa, respectively and were much higher than those of the IE C18:0 30% which were $7.7 \times 10^4 \pm 5.1 \times 10^3$ and 4.2×10^3 ± 324 Pa, respectively. Upon sonication, there was no significant increase in these rheological properties in either of the samples. The phase angle (δ) of the PB and IE C18:0 30% sample were 10.2 ± 0.6 and 3.2 ± 0.1, respectively and these did not change significantly ($p< 0.05$) upon sonication (Figure 8D). Since these values were $0º < \delta < 90º$, both samples were considered viscoelastic.

The rheology data for the IE C18:0 20% and the 30% samples at supercoolings of 9, 6, and 3 ºC are presented in Figure 9. It has been shown by several authors [13, 15, 18] that HIU induces the formation of smaller and more crystals in the system which improves the hardness of the fat. Based on the statistics indicated in Figure 9, it can be seen that sonication significantly increased

the viscosity, G' and the G'' (Figure 9A-C), and decreased δ values for the IE C18:0 20% samples at all the supercooling levels (Figure 9D). For example, the viscosity of the IE C18:0 20% sample increased significantly from 296 ± 32 to 1,606 ± 96 Pa.s and the G' increased significantly from 5,226 ± 429 to 43,893 ± 2,533 Pa upon sonication at ΔT = 6 ºC. The G" of the IE C18:0 20% samples increased significantly from 460 ± 23 to 3,337 ± 380 Pa. This correlates well with the change in the microstructure of the samples upon sonication to smaller crystals which improved the rheological properties of the samples.

The viscosities, G', and the G" of the IE C16:0 20% samples from the previous study [18] were in general lower than those of the IE C18:0 20% samples at all the supercooling levels. This effect may be due to the higher SFC of the C18:0 20% samples compared to the C16:0 20% samples at all the supercoolings [18]. Also, in contrast, sonication did not significantly affect any of the rheological properties of the IE C16:0 20% samples at any of the supercoolings tested. This effect can be associated with the crystallization temperatures of the samples. The IE C16:0 20% samples were crystallized at 7, 10 and 13 ºC [18] while the samples in this study were crystallized at 29, 32 and 35 ºC at supercoolings of 9, 6, and 3 ºC. The lower crystallization temperatures create higher viscosities in the sample during sonication which impedes the formation of cavities in the system. Due to this effect sonication was not very effective in the IE C16:0 20% samples.

The viscosity of the IE C18:0 30% sample increased significantly ($p < 0.05$) at all supercooling levels upon sonication similar to the previous study [18] with the IE C16:0 30% samples (Figure 7E). For example, the viscosity of IE C18:0 30% at ΔT = 6 ºC was 1,901 ± 186 which increased to 6,756 ± 595 Pa.s upon sonication. Along with the final SFC, the viscosity of the IE C18:0 30% samples were also higher than the IE C18:0 20% and IE C16:0 30% [18] at all the supercoolings.

Both G' and the G'' were higher for the IE C18:0 30% samples compared to the IE C18:0 20% and the IE C16:0 30% samples. This effect could be due to the differences in the TAG composition and the presence of higher melting TAGs that give the sample a harder texture or due to the differences in the microstructure. The SFC of the IE C18:0 30% samples were higher than that of the IE C18:0 20% and the IE C16:0 30% samples [18]. While the elastic modulus, G' and the viscous modulus, G'' of the IE C18:0 30% samples did increase upon sonication Figure 9 F-G), the increase in these parameters was not statistically significant ($p > 0.05$). On the other hand, in the previous study [18], the G' and G" of the IE C16:0 30% samples increased significantly at $\Delta T = 3$ ºC upon sonication. Sonication was effective in inducing nucleation and formation of smaller crystals along with changing the melting characteristics of the sample. These changes did increase the viscosity of the sample, however it remains uncertain why the changes in the G' and the G" were not significant. The phase angle (δ) was $0º < \delta < 90º$ indicating that the sample maintained its viscoelastic behavior (Figure 9H).

CONCLUSION

This study shows that HIU affects the crystallization behavior and rheological properties of fats with low content of saturation by not only generating small crystals but also by promoting the induction of crystallization of certain TAG fractions. Tristearin was the highest melting TAG in all the samples and the amount of SSS in the IE samples drove the crystallization behavior and influenced the rheological properties of the samples. Sonication promoted crystallization of low melting TAGs and the incorporation of SSS into the crystalline network.

The IE samples with stearic acid at the *sn*-2 position have superior crystallization properties including SFC and rheology than the IE with palmitic acid at the *sn*-2 position which were evaluated in an earlier study by the same authors. Although HIU was not as effective at inducing

crystallization in the IE C16:0 20% samples due to the lower amount of saturated fats in the system, HIU induced crystallization in both the IE C18:0 20 and 30% samples. This could have been due to the higher melting point of the stearic containing samples compared to the palmitic ones. The induction of superior crystallization properties in these samples upon sonication can make them great candidates as ingredients for *trans*-fat free applications.

ACKNOWLEDGEMENTS: This project was supported by Agriculture and Food Research Initiative (AFRI) Grant no. 2014-67017-21634 from the USDA National Institute of Food and Agriculture, Improving Food Quality – A1361. This project was approved by the Utah Agricultural Experiment Station as project number 8967. The authors would like to thank Maria A. Moore for her help with sample preparation.

REFERENCES

1. Holm HC, Cowan D (2008) The evolution of enzymatic interesterification in the oils and fats industry, European Journal of Lipid Science and Technology 110:679-691

2. Macrae AR (1983) Lipase-catalyzed interesterification of oils and fats, Journal of the American Oil Chemists' Society 60:291-294

3. Ifeduba EA, Martini S, Akoh CC (2016) Enzymatic interesterification of high oleic sunflower oil and tripalmitin or tristearin, Journal of the American Oil Chemists' Society 93:61-67

4. Yli-Jokipii K, Kallio H, Schwab U, Mykkänen H, Kurvinen J-P, Savolainen MJ, Tahvonen R (2001) Effects of palm oil and transesterified palm oil on chylomicron and VLDL

triacylglycerol structures and postprandial lipid response, Journal of Lipid Research 42:1618-1625

5. Robinson DM, Martin NC, Robinson LE, Ahmadi L, Marangoni AG, Wright AJ (2009) Influence of interesterification of a stearic acid-rich spreadable fat on acute metabolic risk factors, Lipids 44:17-26

6. Yli-Jokipii KM, Schwab US, Tahvonen RL, Kurvinen J-P, Mykkänen HM, Kallio HPT (2003) Chylomicron and VLDL TAG structures and postprandial lipid response induced by lard and modified lard, Lipids 38:693-703

7. Hall WL, Iqbal S, Li H, Gray R, Berry SEE (2016) Modulation of postprandial lipaemia by a single meal containing a commonly consumed interesterified palmitic acid-rich fat blend compared to a non-interesterified equivalent, European Journal of Nutrition:1-9

8. Rousseau D, Marangoni AG (1998) Tailoring the textural attributes of butter fat/canola oil blends via rhizopus arrhizus lipase-catalyzed interesterification. 2. Modifications of physical properties, Journal of Agricultural and Food Chemistry 46:2375-2381

9. Fauzi SHM, Rashid NA, Omar Z (2013) Effects of enzymatic interesterification on the physicochemical, polymorphism and textural properties of palm stearin, palm kernel oil and soybean oil blends, International Journal of Bioscience, Biochemistry and Bioinformatics 3:398

10. Yu D, Liu B, Wang B (2012) The effect of ultrasonic waves on the nucleation of pure water and degassed water, Ultrasonics Sonochemistry 19:459-463

11. Kiani H, Zhang Z, Delgado A, Sun D-W (2011) Ultrasound assisted nucleation of some liquid and solid model foods during freezing, Food Research International 44:2915-2921

12. Higaki K, Ueno S, Koyano T, Sato K (2001) Effects of ultrasonic irradiation on crystallization behavior of tripalmitoylglycerol and cocoa butter, Journal of the American Oil Chemists' Society 78:513-518

13. Suzuki A, Lee J, Padilla S, Martini S (2010) Altering functional properties of fats using power ultrasound, Journal of Food Science 75:E208-E214

14. Martini S, Suzuki AH, Hartel RW (2008) Effect of high intensity ultrasound on crystallization behavior of anhydrous milk fat, Journal of the American Oil Chemists' Society 85:621-628

15. Ye Y, Wagh A, Martini S (2011) Using high intensity ultrasound as a tool to change the functional properties of interesterified soybean oil, Journal of Agricultural and Food Chemistry 59:10712-10722

16. Ye Y (2015) Effect of High Intensity Ultrasound on Crystallization Behavior and Functional Properties of Lipids, All Graduate Theses and Dissertations. Paper 4281

17. Chen F, Zhang H, Sun X, Wang X, Xu X (2013) Effects of ultrasonic parameters on the crystallization behavior of palm oil, Journal of the American Oil Chemists' Society 90:941-949

18. Kadamne JV, Ifeduba EA, Akoh CC, Martini S (2017) Sonocrystallization of interesterified fats with 20 and 30% C16:0 at s*n*-2 position, Journal of the American Oil Chemists' Society 94:3-18

19. Wagh A, Walsh MK, Martini S (2013) Effect of lactose monolaurate and high intensity ultrasound on crystallization behavior of anhydrous milk fat, Journal of the American Oil Chemists' Society 90:977-987

20. Foubert I, Dewettinck K, Vanrolleghem PA (2003) Modelling of the crystallization kinetics of fats, Trends in Food Science & Technology 14:79-92

21. Belitz H-D, Grosch W, Schieberle P (2013) Lipids. Food Chemistry. Springer, Berlin Heidelberg, pp. 157-244.

22. Herrera ML, Hartel RW (2000) Effect of processing conditions on crystallization kinetics of a milk fat model system, Journal of the American Oil Chemists' Society 77:1177-1188

23. Martini S, Herrera ML, Hartel RW (2002) Effect of processing conditions on microstructure of milk fat fraction/sunflower oil blends, Journal of the American Oil Chemists' Society 79:1063-1068

24. Wu L, Cao J, Bai X, Chen H, Zhang Y, Wu Q (2016) Effects of Ultrasonic Parameters on the Crystallization Behavior of Virgin Coconut Oil, Journal of Oleo Science 65:967-976

FIGURE CAPTIONS

Figure 1: Solid Fat content of the IE and PB C18:0 20% and 30% samples at ΔT= 12 °C. The point of application of HIU for the PB sample is indicated with a dotted arrow on the time axis while that of the IE samples is indicated with a solid arrow. Mean values and standard errors of three experimental replicates are reported.

Figure 2: Solid Fat Content of IE C18:0 20% and 30% samples at ΔT= 9, 6, and 3 °C. The point of application of HIU is indicated with an arrow on the time axis. Mean values and standard errors of three experimental replicates are reported.

Figure 3: PLM of sonicated and non-sonicated IE and PB C18:0 20% and 30% at ΔT = 12 °C after 60 minutes of crystallization. (The white bar represents 100 µm)

Figure 4: PLM of sonicated and non-sonicated IE and PB C18:0 20% at ΔT = 9, 6 and 3 °C after 60 minutes of crystallization. (The white bar represents 100 µm)

Figure 5: PLM of sonicated and non-sonicated IE and PB C18:0 30% at ΔT = 9, 6 and 3 °C after 60 minutes of crystallization. (The white bar represents 100 µm)

Figure 6: DSC thermograms of sonicated and non-sonicated IE and PB C18:0 20% and 30% at ΔT = 12 °C

Figure 7: DSC thermograms of sonicated and non-sonicated IE C18:0 20% and 30% at ΔT = 9, 6 and 3 °C

Figure 8: Rheology parameters, viscosity, G', G'' and of sonicated and non-sonicated IE and PB C18:0 20% and 30% at ΔT = 12 °C. Mean values and standard errors of three experimental replicates are reported. For samples within each group (C18:0 20% or C18:0 30%), parameters with different alphabets are statistically different (α = 0.05)

Figure 9: Rheology parameters, viscosity, G', G'' and of sonicated and non-sonicated IE C18:0 20% and IE C18:0 30% at ΔT = 9, 6 and 3 °C. Mean values and standard errors of three experimental replicates are reported. Parameters at each supercooling represented with different alphabets are statistically different (α =0.05)

Table 1: Melting point (T_m), crystallization temperatures (T_c), melting enthalpy (ΔH) and the driving force of crystallization (ϕ) at different supercooling levels

Sample	T_m (°C)	ΔH (J/g)	ΔT = 12 °C		ΔT = 9 °C		ΔT = 6 °C		ΔT = 3 °C	
			T_c (°C)	ϕ (J/g)	T_c (°C)	ϕ (J/g)	T_c (°C)	ϕ (J/g)	T_c (°C)	ϕ (J/g)
PB C18:0 20%	53.6 ± 0.4	105.2 ± 1.8	42.0	23.6	45.0	17.7	48.0	11.8	51.0	5.9
IE C18:0 20%	38.0 ± 0.3	106.5 ± 2.2	26.0	33.6	29.0	25.2	32.0	16.8	35.0	8.4
PB C18:0 30%	60.0 ± 0.4	126.4 ± 1.6	48.0	25.3	51.0	19.0	54.0	12.6	57.0	6.3
IE C18:0 30%	43.2 ± 0.6	105.2 ± 1.3	31.0	29.2	34.0	21.9	37.0	14.6	40.0	7.3

Table 2: Total and *sn*-2 fatty acid composition of IE C18:0 20% and IE C18:0 30% samples

	Total fatty acid composition (mol%)							
Sample	**C16:0**	**C18:0**	**C18:1n9**	**C18:2n6**	**C20:1**	**C21:0**	**C22:1n9**	**C24:1**
IE C18:0 20*	4.9 ± 0.0	19.2 ± 0.1	70.2 ± 0.6	4.1 ± 0.6	0.2 ± 0.0	ND	0.9 ± 0.0	0.3 ± 0.0
IE C18:0 30*	5.9 ± 0.1	28.3 ± 1.5	60.7 ± 1.1	3.2 ± 0.2	0.3 ± 0.0	0.2 ± 0.0	0.9 ± 0.0	0.3 ± 0.0

	Positional (*sn*-2) fatty acid composition (mol%)			
Sample	**C16:0**	**C18:0**	**C18:1n9**	**C18:2n6**
IE C18:0 20%	2.5 ± 0.5	17.0 ± 0.4	75.3 ± 1.6	5.2 ± 0.7
IE C18:0 30%	3.2 ± 0.2	33.2 ± 0.1	60.0 ± 0.2	3.6 ± 0.3

**Trace amounts of C14:0 and C15:0*
Mean ± SD, n =2
ND not detected

Table 3: Triacylglycerol (TAG) composition of the IE C18:0 20% and the IE C18:0 30%

	TAG Molecular Species (peak area %)				
Sample	**LOO + LPO**	**OOO**	**OOS**	**OSS**	**SSS**
IE C18:0 20%	2.1 ± 0.1	69.0 ± 0.3	23.7 ± 0.4	4.0 ± 0.1	1.2 ± 0.1
IE C18:0 30%	0.9 ± 0.1	39.9 ± 0.8	42.7 ± 1.0	14.3 ± 0.1	2.3 ± 0.2

Table 4: Gompertz parameters –Maximum SFC (s_{max}), rate of crystallization (μ) and Induction period (λ) obtained from the Gompertz fit to the solid fat content data of the sonicated and non-sonicated IE and PB samples

	Gompertz Parameters	IE- no HIU	IE- with HIU	PB- no HIU	PB- with HIU
C18:0 20% samples					
ΔT = 12 °C	**s_{max} (%)**	8.56 ± 0.07^{c}	8.62 ± 0.06^{c}	13.54 ± 0.11^{a}	13.08 ± 0.11^{b}
	μ (%SFC/min)	0.98 ± 0.07^{b}	0.90 ± 0.05^{b}	3.33 ± 0.30^{b}	10.12 ± 2.22^{a}
	λ (min)	2.07 ± 0.29^{b}	2.15 ± 0.25^{b}	7.33 ± 0.20^{a}	6.53 ± 0.14^{a}
ΔT = 9 °C	**s_{max} (%)**	7.51 ± 0.05^{a}	7.62 ± 0.04^{a}		
	μ (%SFC/min)	0.89 ± 0.05^{b}	1.18 ± 0.06^{a}		
	λ (min)	3.99 ± 0.21^{a}	4.33 ± 0.15^{a}		
ΔT = 6 °C	**s_{max} (%)**	6.44 ± 0.04^{a}	6.51 ± 0.02^{a}		
	μ (%SFC/min)	0.76 ± 0.04^{b}	1.61 ± 0.08^{a}		
	λ (min)	9.36 ± 0.22^{a}	8.39 ± 0.10^{b}		
ΔT = 3 °C	**s_{max} (%)**	5.52 ± 0.05^{a}	5.55 ± 0.02^{a}		
	μ (%SFC/min)	0.46 ± 0.03^{b}	1.54 ± 0.08^{a}		
	λ (min)	13.03 ± 0.40^{b}	11.77 ± 0.11^{a}		
C18:0 30% samples					
ΔT = 12 °C	**s_{max} (%)**	10.81 ± 0.06^{b}	10.74 ± 0.06^{b}	18.21 ± 0.15^{a}	18.01 ± 0.12^{a}
	μ (%SFC/min)	0.79 ± 0.03^{c}	0.84 ± 0.03^{c}	3.24 ± 0.23^{b}	4.84 ± 0.37^{a}
	λ (min)	2.17 ± 0.27^{c}	2.76 ± 0.28^{c}	11.91 ± 0.21^{a}	8.71 ± 0.16^{b}
ΔT = 9 °C	**s_{max} (%)**	9.00 ± 0.08^{a}	9.05 ± 0.04^{a}		
	μ (%SFC/min)	0.66 ± 0.03^{b}	1.38 ± 0.06^{a}		
	λ (min)	9.41 ± 0.37^{a}	9.56 ± 0.14^{a}		
ΔT = 6 °C	**s_{max} (%)**	7.17 ± 0.05^{a}	7.37 ± 0.05^{a}		
	μ (%SFC/min)	0.48 ± 0.02^{b}	0.93 ± 0.05^{a}		
	λ (min)	15.55 ± 0.27^{a}	14.13 ± 0.21^{a}		
ΔT = 3 °C	**s_{max} (%)**	5.19 ± 0.27^{a}	5.58 ± 0.09^{a}		
	μ (%SFC/min)	0.17 ± 0.01^{b}	0.43 ± 0.04^{a}		
	λ (min)	29.30 ± 0.53^{a}	21.39 ± 0.60^{b}		

At ΔT = 12 °C, each parameter viz. smax, μ and λ was compared between the IE and PB (sonicated and non-sonicated samples) for both the IE C18:0 20 and 30% samples by a 2-way ANOVA followed by Tukeys' multiple comparison test. At ΔT = 9, 6 and 3 °C, each was compared among all the supercooling by 2-way ANOVA followed by Sidak's multiple comparison between the sonicated and the non-sonicated samples at each supercooling separately.

Table 5: DSC melting parameters $T_{on,}$ T_p and enthalpy (ΔH) for the interesterified (IE) samples and physical blends (PB) at ΔT = 12 °C. Each parameter is compared between the sonicated and non-sonicated PB and IE within the same group (C18:0 20% or C18:0 30%). The parameters represented with different alphabets are statistically different (α = 0.05)

		PB C18:0 20%				IE C18:0 20%		
		T_{on} (°C)	T_p (°C)	ΔH (J/g)		T_{on} (°C)	T_p (°C)	ΔH (J/g)
Peak 1	**No HIU**	53.3 ± 1.0[a]	61.2 ± 0.4[a]	33.8 ± 1.8[a]		39.8 ± 0.4[b]	52.8 ± 0.1[b]	9.2 ± 0.5[b]
	With HIU	53.0 ± 0.6[a]	61.4 ± 0.1[a]	36.3 ± 1.4[a]		40.3 ± 0.4[b]	52.7 ± 0.1[b]	9.4 ± 0.1[b]

		PB C18:0 30%				IE C18:0 30%		
		T_{on} (°C)	T_p (°C)	ΔH (J/g)		T_{on} (°C)	T_p (°C)	ΔH (J/g)
Peak 1	**No HIU**	54.0 ± 1.3[a]	58.1 ± 0.7[a]	21.9 ± 3.8[a]		38.2 ± 0.6[b]	43.1 ± 0.4[b]	2.1 ±0.2[b]
	With HIU	52.1 ± 0.1[a*]	57.3 ±0.6[a]	36.1 ± 7.1[a]		37.9 ± 0.6[b]	43.4 ± 0.3[b]	2.7 ± 0.2[b]
Peak 2	**No HIU**	61.8 ± 0.9[a]	64.9 ± 0.5[a]	10.8 ± 4.8[a]		47.6 ± 0.2[b]	54.0 ± 0.1[b]	4.5 ± 0.2[a]
	With HIU	60.8 ± 0.6[a]	64.9 ± 0.2[a]	13.0 ± 5.3[a]		48.1 ± 0.4[b]	53.3 ± 0.1[b]	3.7 ± 0.4[a]

* The Ton temperature of only two replicates were calculated by the software

Table 6: DSC melting parameters $T_{on,}$ T_p and enthalpy (ΔH) for the interesterified (IE) samples C18:0 20% and 30% at ΔT = 9, 6 and 3 °C. Within a sample each parameter is compared between the sonicated and non-sonicated sample at each supercooling. The parameters represented with different superscripts are statistically different ($\alpha = 0.05$)

IE C18:0 20%								
ΔT (°C)		**Peak 1**				**Peak 2**		
		T_{on} (°C)	**T_p (°C)**	**ΔH (J/g)**		**T_{on} (°C)**	**T_p (°C)**	**ΔH (J/g)**
9	**No HIU**	ND*	ND*	ND*		42.4 ± 0.2[b]	53.1 ± 0.4[a]	6.8 ± 0.3[a]
	With HIU	37.7 ± 0.4	41.2 ± 0.7	0.8 ± 0.6		46.3 ± 0.4[a]	53.4 ± 0.2[a]	4.1 ± 0.2[b]
6	**No HIU**	ND*	ND*	ND*		46.0 ± 1.3[b]	54.2 ± 0.1[a]	4.2 ± 0.7[a]
	With HIU	41.5 ± 1.5	44.7 ± 0.3	4.9 ± 0.6		49.2 ± 0.3[a]	53.6 ± 0.2[a]	2.9 ± 0.4[a]
3	**No HIU**	42.7 ± 0.4[a]	47.8 ± 0.1[a]	1.0 ± 0.4[a]		52.5 ± 0.4[a]	55.9 ± 0.4[a]	1.2 ± 0.2[a]
	With HIU	42.5 ± 0.6[a]	46.5 ± 0.3[a]	6.4 ± 0.034[b]		53.6 ± 0.4[a]	55.7 ± 0.2[a]	0.1 ± 0.1[a]
IE C18:0 30%								
ΔT (°C)		**Peak 1**				**Peak 2**		
		T_{on} (°C)	**T_p (°C)**	**ΔH (J/g)**		**T_{on} (°C)**	**T_p (°C)**	**ΔH (J/g)**
9	**No HIU**	39.9 ± 0.5	45.2 ± 0.3[b]	3.8 ± 0.6[b]		50.3 ± 0.3[b]	54.5 ± 0.3[a]	2.6 ± 0.8[a]
	With HIU	43.3**	46.3 ± 0.2[a]	13.0 ± 0.3[a]		53.3 ± 0.3[a]	55.1 ± 0.1[a]	0.1 ± 0.04[b]
6	**No HIU**	N/A***	48.6 ± 0.3[a]	11.3 ± 0.8[a]		55.2 ± 0.7	57.3 ± 0.3	0.1 ± 0.1
	With HIU	N/A***	47.3 ± 0.1[b]	12.9 ± 0.5[a]		ND	ND	ND
3	**No HIU**	43.3**	51.0 ± 0.3[a]	9.4 ± 1.0[b]		ND	ND	ND
	With HIU	41.2 ± 0.002****	48.0 ± 0.1[b]	12.9 ± 0.3[a]		ND	ND	ND

* certain peaks were not detected at all the processing conditions; ** The T_{on} temperature of only one replicate was calculated by the software; *** For peaks where the T_{on} temperature could not be determined by the software, it is denoted by N/A; **** The T_{on} temperature of only two replicates was calculated by the software

Figure 1: Solid Fat content of the IE and PB C18:0 20% and 30% samples at ΔT= 12 °C. The point of application of HIU for the PB sample is indicated with a dotted arrow on the time axis while that of the IE samples is indicated with a solid arrow. Mean values and standard errors of three experimental replicates are reported.

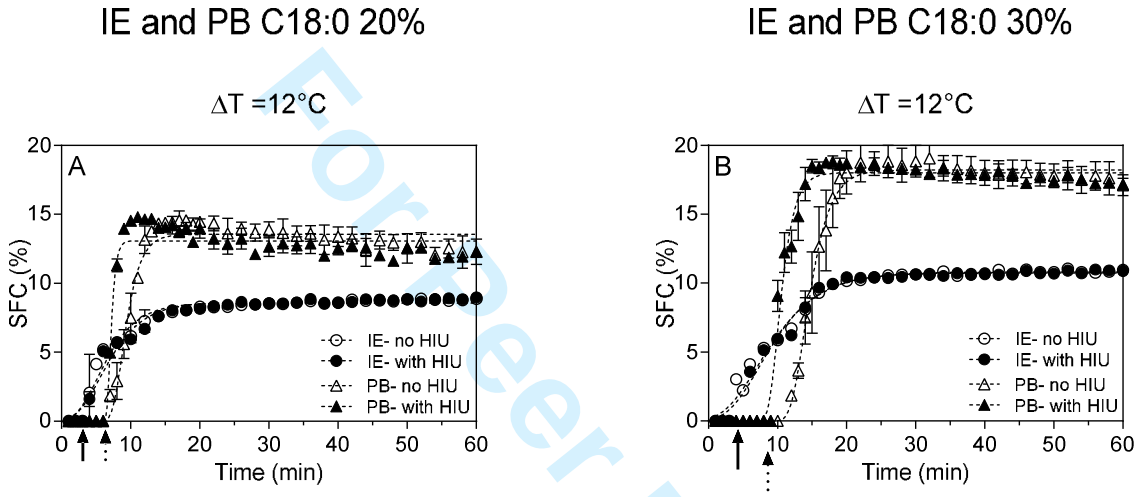

Figure 2: Solid Fat Content of IE C18:0 20% and 30% samples at ΔT= 9, 6, and 3 °C. The point of application of HIU is indicated with an arrow on the time axis. Mean values and standard errors of three experimental replicates are reported.

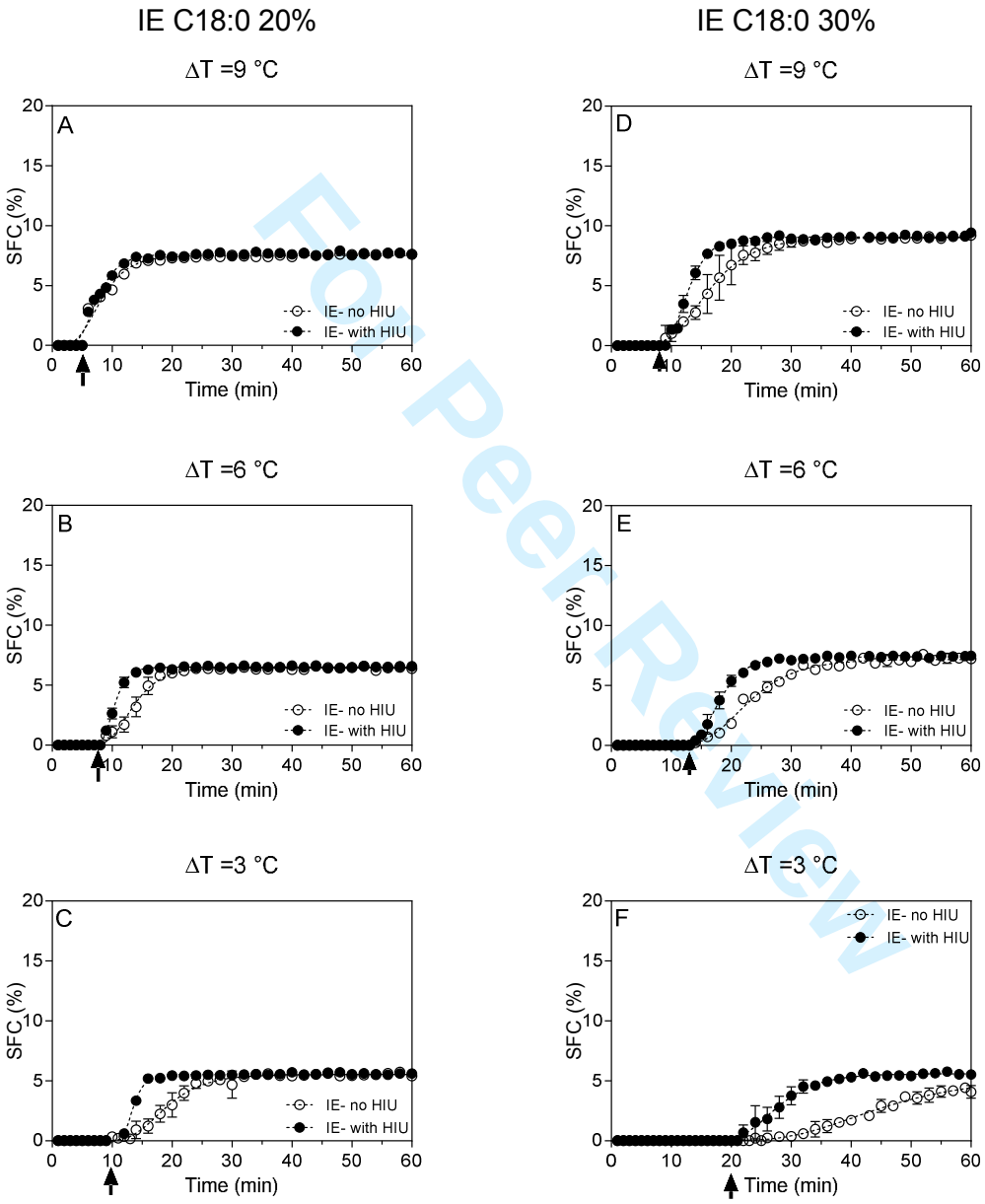

Figure 3: PLM of sonicated and non-sonicated IE and PB C18:0 20% and 30% at ΔT = 12 °C after 60 minutes of crystallization. (The white bar represents 100 μm)

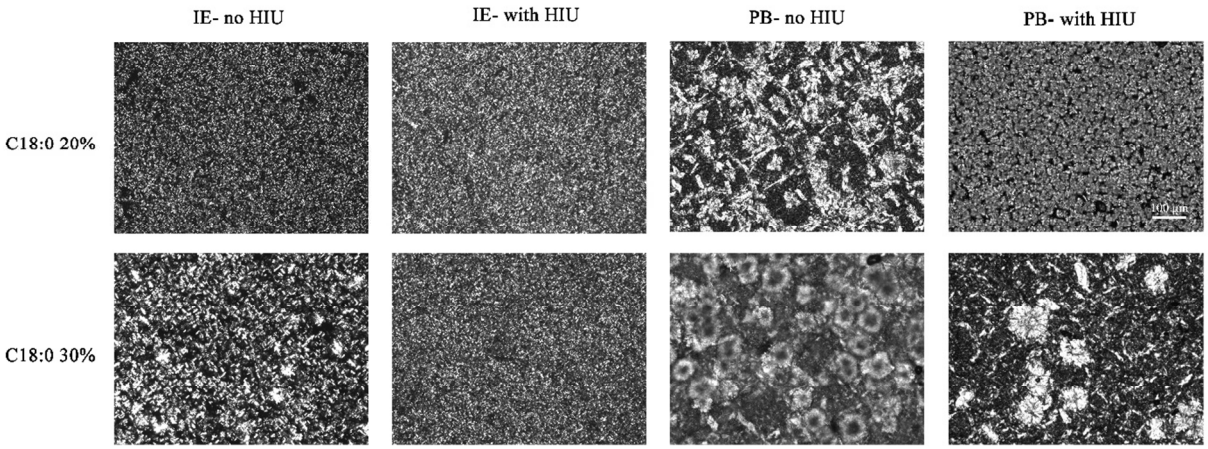

Figure 4: PLM of sonicated and non-sonicated IE and PB C18:0 20% at ΔT = 9, 6 and 3 °C after 60 minutes of crystallization. (The white bar represents 100 μm)

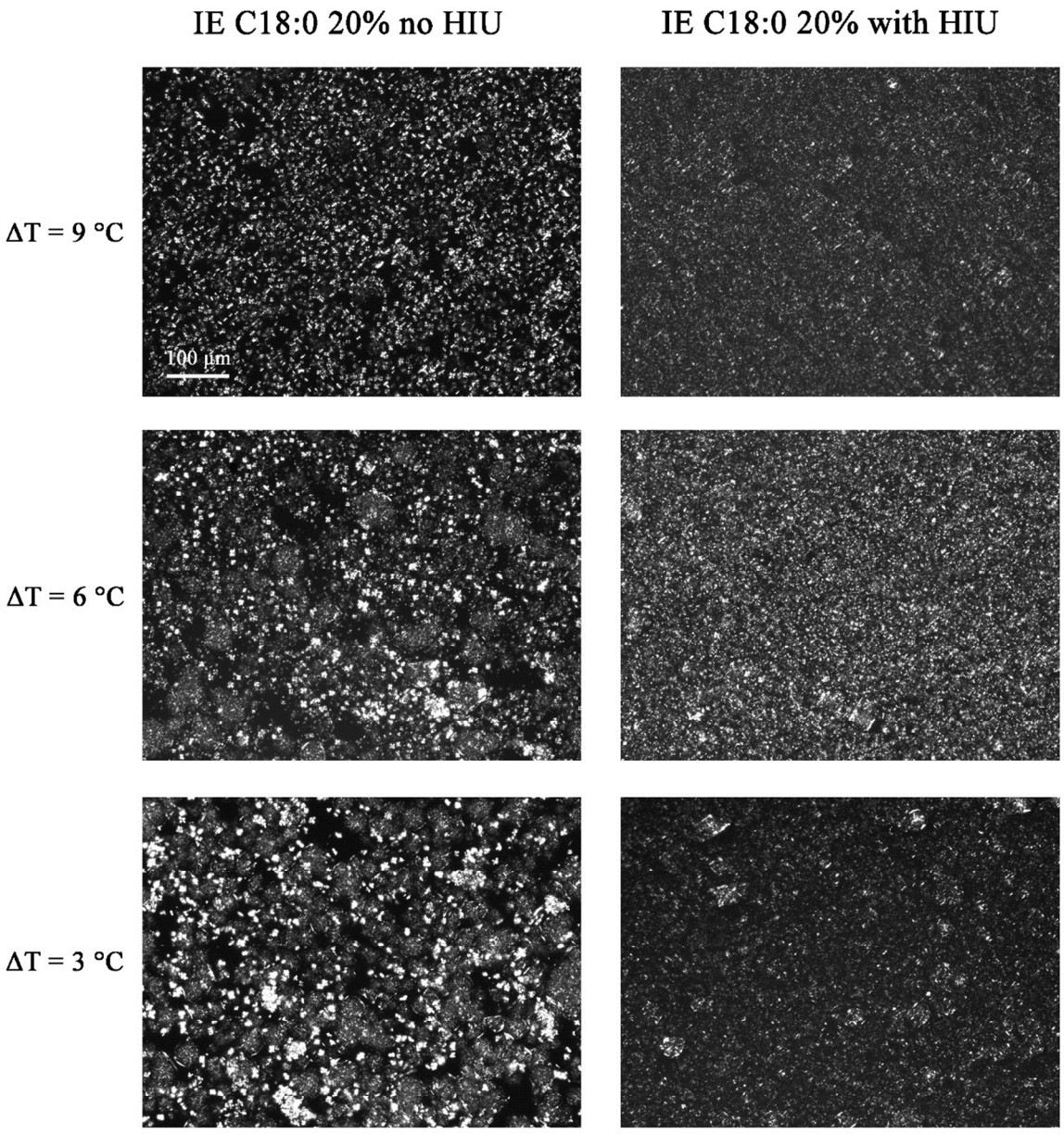

Figure 5: PLM of sonicated and non-sonicated IE and PB C18:0 30% at ΔT = 9, 6 and 3 °C after 60 minutes of crystallization. (The white bar represents 100 μm)

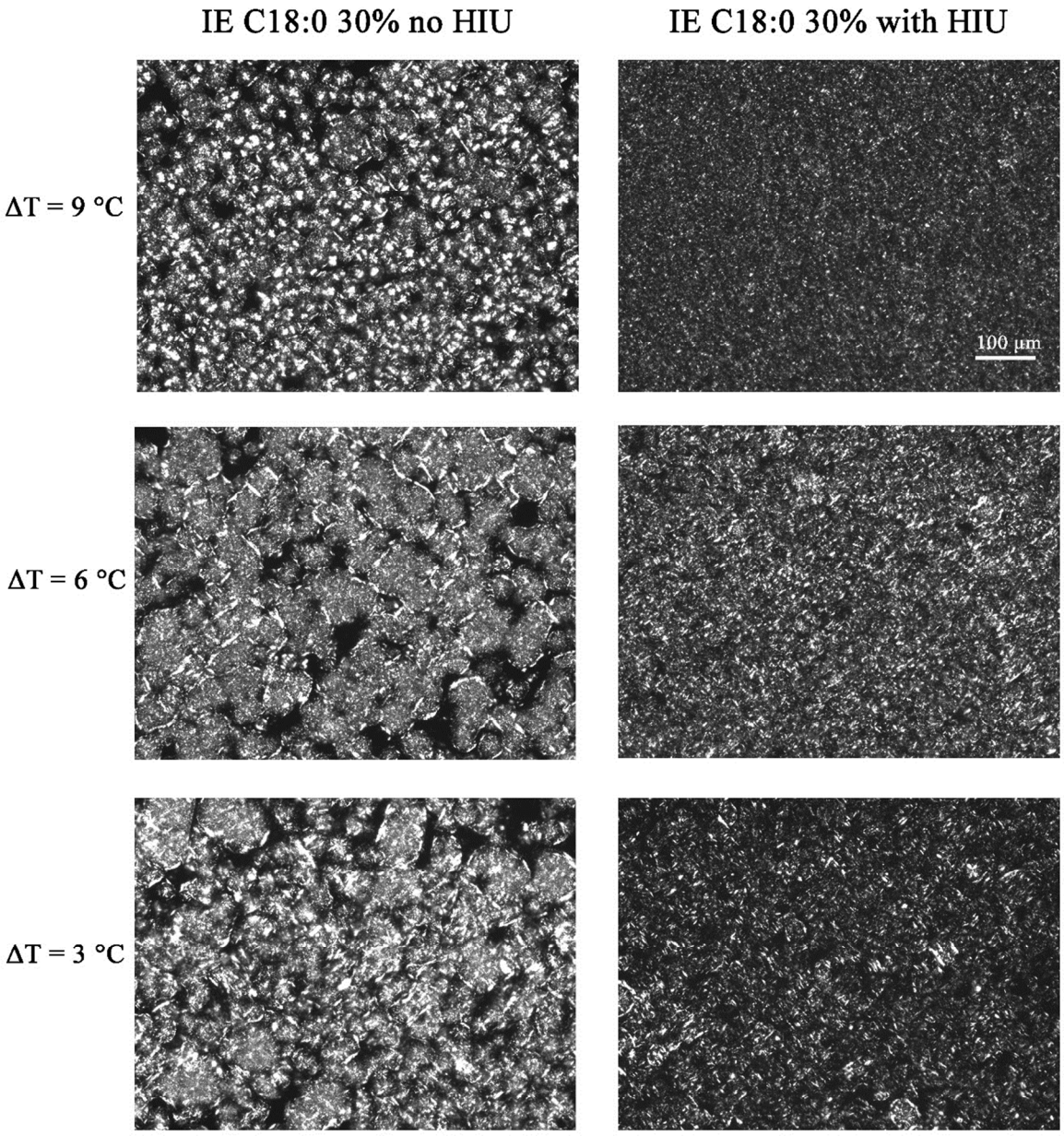

Figure 6: DSC thermograms of sonicated and non-sonicated IE and PB C18:0 20% and 30% at ΔT = 12 °C

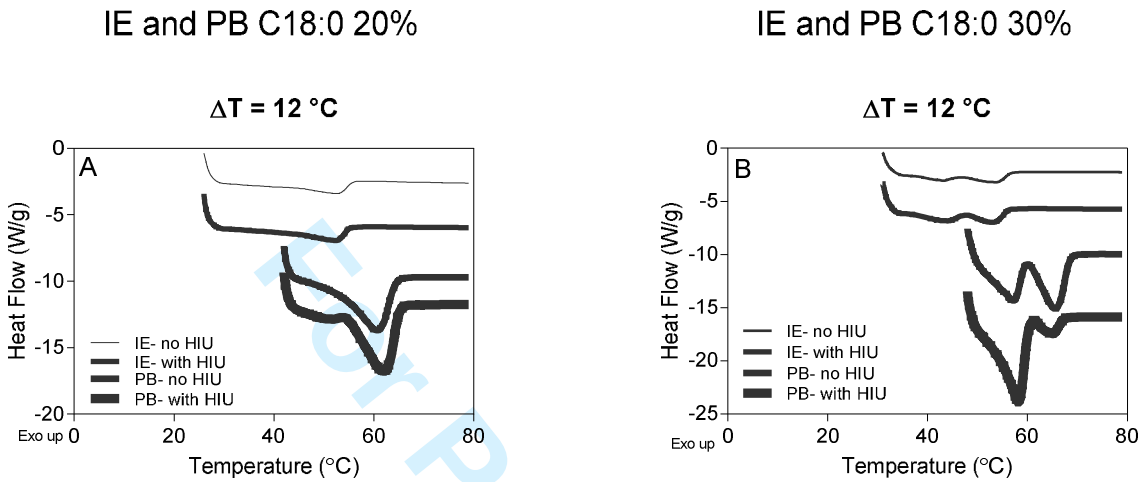

Figure 7: DSC thermograms of sonicated and non-sonicated IE C18:0 20% and 30% at ΔT = 9, 6 and 3 °C

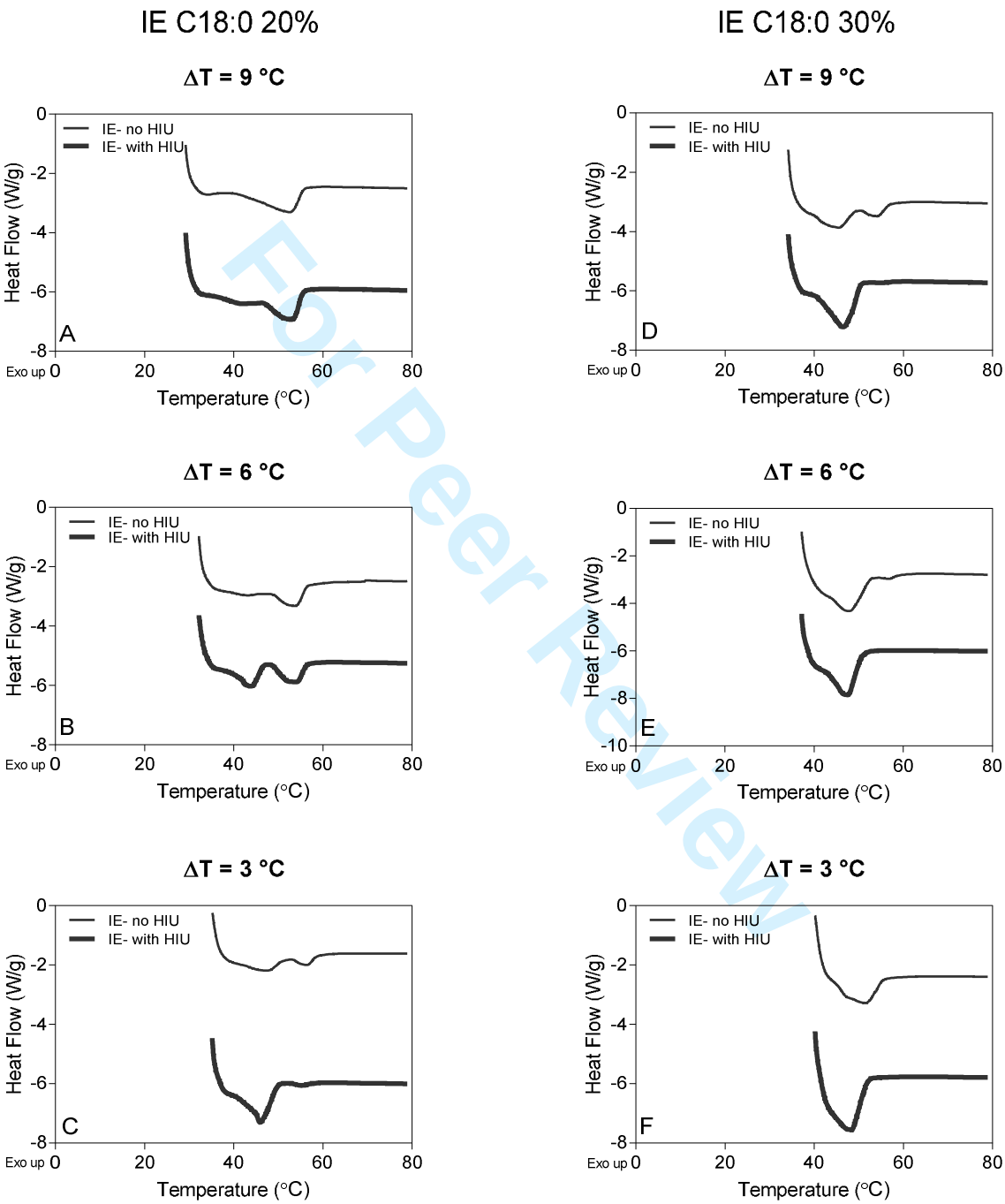

Figure 8: Rheology parameters, viscosity, G', G'' and of sonicated and non-sonicated IE and PB C18:0 20% and 30% at ΔT = 12 °C. Mean values and standard errors of three experimental replicates are reported. For samples within each group (C18:0 20% or C18:0 30%), parameters with different alphabets are statistically different (α = 0.05)

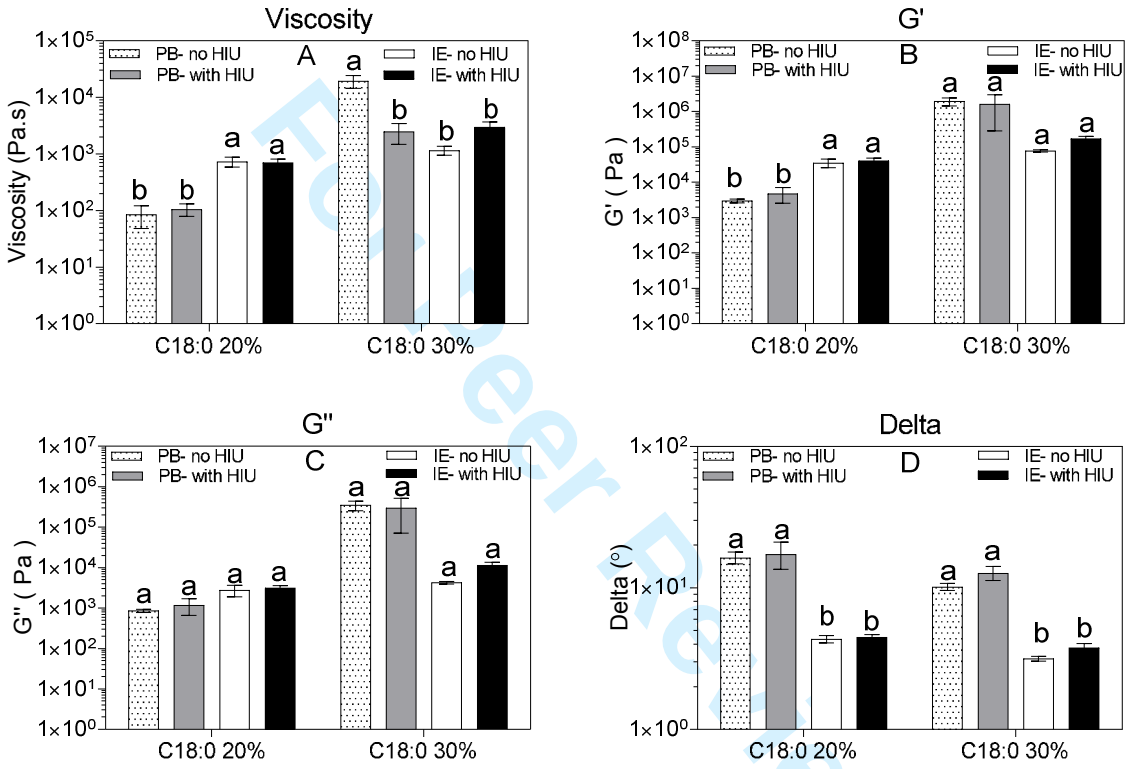

Figure 9: Rheology parameters, viscosity, G', G'' and of sonicated and non-sonicated IE C18:0 20% and IE C18:0 30% at ΔT = 9, 6 and 3 °C. Mean values and standard errors of three experimental replicates are reported. Parameters at each supercooling represented with different alphabets are statistically different (α =0.05)